Short-Range FMCW Monopulse Radar for Hand-Gesture Sensing

Pavlo Molchanov, Shalini Gupta, Kihwan Kim, and Kari Pulli

NVIDIA Research, Santa Clara, California, USA

Abstract—**Intelligent driver assistance systems have become important in the automotive industry. One key element of such systems is a smart user interface that tracks and recognizes drivers' hand gestures. Hand gesture sensing using traditional computer vision techniques is challenging because of wide variations in lighting conditions, *e.g.* inside a car. A short-range radar device can provide additional information, including the location and instantaneous radial velocity of moving objects. We describe a novel end-to-end (hardware, interface, and software) short-range FMCW radar-based system designed to effectively sense dynamic hand gestures. We provide an effective method for selecting the parameters of the FMCW waveform and for jointly calibrating the radar system with a depth sensor. Finally, we demonstrate that our system guarantees reliable and robust performance.**

I. INTRODUCTION

Hand gestures are a natural form of human communication. In automobiles, a gesture-based user interface can improve drivers' safety. It allows drivers to focus on driving while interacting with the infotainment or controls (*e.g.*, air conditioning) in the car. A short-range radar sensor can add extra modalities to gesture tracking/recognition systems. One of these modalities is the instantaneous radial velocity of the driver's moving hand. Advantages of the radar system are (1) robustness to lighting conditions compared to other sensors, (2) low computational complexity due to direct detection of moving objects, and (3) occlusion handling because of the penetration capability of EM waves.

Prior work in hand gesture recognition primarily used depth and optical sensors [1]. Optical sensors do not provide accurate depth estimation, and depth sensors can be unreliable outdoors where sunlight corrupts their measurements. Technically time-of-flight (TOF) depth and radar sensors are similar, as they both measure the delay of the signal traveling to and from the object. However, radar sensors use lower frequencies, which allows for the estimation of the phase of the wave and consequently the Doppler shift. Using radar-like sensors for gesture sensing has been studied recently [2], [3], [4]. In most of these works, the hand is modeled as a single rigid object. However, in reality, it is not and in this work we model the hand as a non-rigid object. This allows us to perceive the hand as a multi-scatterer object and to capture its local micro-motions.

In this work, we describe a novel end-to-end (hardware, interface, and software) short-range radar-based system designed and prototyped to effectively measure dynamic hand gestures (see Fig. 1). The idea behind the proposed radar system for gesture recognition is the fact that the hand behaves as a non-rigid object. Therefore, in the context of dynamic gesture recognition, a hand gesture produces a multiple reflections
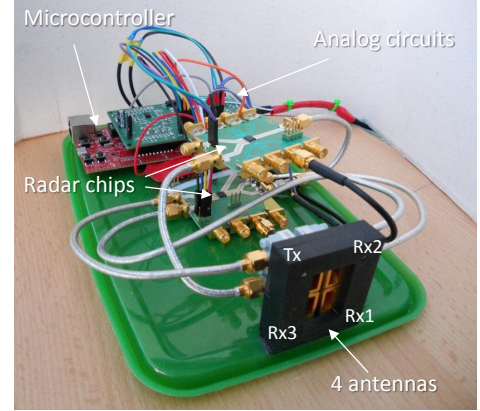

Fig. 1: A short-range monopulse FMCW radar prototype built for gesture sensing (left). The black plastic component encases four rectangular waveguide antennas (SMA to WR42 adapters).

from different parts of the hand with different range and velocity values that vary over time. Because of this, different dynamic hand gestures produce unique range-Doppler-time representations, which can be employed to recognize them.

We found that Frequency Modulated Continuous Wave (FMCW) radar with multiple receivers (monopulse) is best suited for hand gesture sensing. It can estimate the range and velocity of scatterers, and the angle of arrival of objects that are separated in the range-Doppler map. The information from monopulse FMCW radar is also easier to fuse with depth sensors, because they provide spatial information of the object in 3-dimensions (3D). We used three receivers and the monopulse technique for estimating the azimuth and elevation angles of moving objects, which enabled our system to estimate the spatial location of objects and their radial velocity.

To the best of our knowledge, our radar-based solution for hand gesture sensing is the first of its kind. Our system is similar to long-range radars currently employed in automobiles to sense external environments, but for our solution, which was designed to operate inside a car, we adapted these radar principles to the short-range ($< 1m$) scenario.

The proposed radar system is part of a multi-sensor system for drivers' hand-gesture recognition [5]. In this paper we describe in detail the design and signal processing procedures of the radar system.

The paper is organized as follows. In the Section II, we describe the design and implementation of our proposed radar system. Experiments to validate the radar system's operation with measurements of a disk, a pendulum and a hand are presented in Section III. We conclude the paper in Section IV.
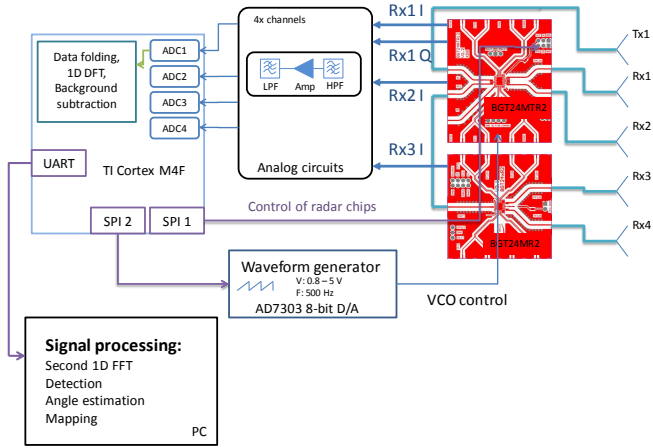
Fig. 2: The block diagram of our short-range radar system for in-car gesture sensing. The system is based on the radar front-end BGT24MTR12 chip by Infineon Technologies. A Cortex M4F micro-controller by Texas Instruments Incorporated does sampling and basic signal processing.

II. METHODOLOGY

A. Design

Fig. 2 illustrates the block diagram of our short-range radar system. The system uses a FMCW radar with multiple receivers. It operates in K-band with central frequency $25GHz$ and bandwidth $4GHz$. It measures a 4D vector (xyz + radial velocity) of each moving object that is detected within its field of view (FOV). It employs the Doppler effect to measure the velocity of the target moving object, *e.g.*, a hand. It computes the range between the sensor and the object by measuring the beat frequency which is proportional to the time delay of the signal traveling to and from the object. The range and velocity form a range-Doppler map (RDM), where each moving object is localized. Using three receivers, we estimate the azimuth and elevation angles of moving objects by measuring the pair-wise phase differences between the signals at multiple receivers.

The front-end interface of the device employs an Infineon BGT24MTR12 chip, which generates the signal, and frequency modulates/demodulates it. We amplify and demodulate the baseband modulated signal via a custom analog circuit designed to operate in the short-range ($< 1m$). We sample the analog signal, at a rate of 40 KHz, and pre-process it on a programmed TI Tiva Cortex M4F micro-controller. The pre-processing steps include static background subtraction (by a moving target indication (MTI) filter), 1D FFT, and package creation for transmission to the host machine by a UART-to-USB chip. The prototype of the radar system consumes less than $1W$ of power from the USB port only, but the power consumption can be significantly reduced for a packaged product. On the host machine, we estimate the RDM, detect moving objects via a constant false alarm rate (CFAR) detector, estimate their 3D position and velocity, register the radar data to other sensors, and perform application-specific
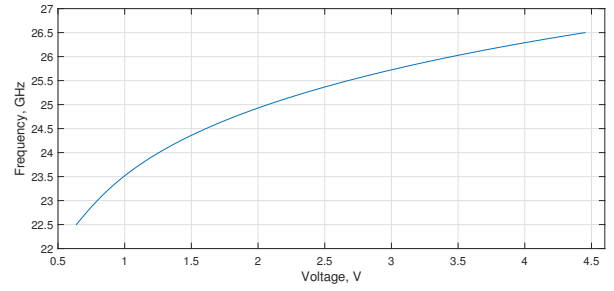

Fig. 3: The measured non-linear voltage-frequency response of the BGT24MTR12 chip, which required chirp linearization.

operations.

Our prototype system is shown in Fig. 1. We designed the system to operate in near real-time. It updates a full set of measurements (range, velocity, azimuth and elevation) for spatially separated objects 32 frames per second. The default output power of the radar is reduced by $9dB$ and is equal to $3dBm$.

B. Chirp linearization

The voltage controlled oscillator (VCO) of the BGT24MTR12 has a non-linear voltage-frequency response shown in Fig. 3. Such behavior is common for VCOs, but for correct operation of the FMCW radar the output of the VCO should be a signal with monotonically increasing frequency. This can be achieved by a specially designed control signal, which compensates for the non-linearly of the voltage-frequency response. We approximated the non-linear voltage-frequency response by a 5th order polynomial and calculated the voltage values for which the frequency output was monotonic between 22.5 and 26.5 GHz. The linearized chirp signal is shown in Fig. 6. We found that linearization was essential for radar-based short-range gesture sensing.

C. Range-Doppler Estimation

We estimated the range and velocity of moving objects by processing the demodulated radar signal. Fig. 4 illustrates the general scheme of range-Doppler processing.

In the FMCW radar, the transmitted signal is frequency modulated by a periodic saw-wave function. The received wave is subject to a frequency shift (Doppler shift, f_d), and is also subject to a time delay τ. The relative motion of the object with respect to the radar causes the Doppler shift. The signal traveling to and from the object causes the time delay (non-zero beat frequency). For saw-wave modulation, the frequency shift and beat frequency are coupled and are difficult to separate for multiple objects.

We decoupled them by processing the range-Doppler maps. We transmitted a number of modulation periods (sweeps), multiplied their responses, and low-pass filtered the resulting signal. We further analyzed the resulting beat signal. We organized it in the form of a matrix, where each column of the matrix contained the beat signal of a single sweep. The

signal is a superposition of reflections from multiple objects I, and has the following form:

$$s(t, n) = \sum_{i=0}^{I} A^{(i)} e^{j(2\pi k\tau^{(i)}t + 2\pi f_d^{(i)}n + \phi^{(i)})}, \qquad (1)$$

where $A^{(i)}$ is the amplitude of the received signal reflected by object i, k is the wave number, $\tau^{(i)}$ is the time delay caused by signal propagation, $f_d^{(i)}$ is the frequency Doppler shift caused by the relative motion of the object, $\phi^{(i)}$ is a linear phase term, t is the fast-time index (samples within a single sweep), and n is the slow-time index (index of the sweep's period). The 2D signal $s(t, n)$ is of size $L \times N$, where L is the number of samples in a single period of a sweep, and N is the number of sweeps considered for range-Doppler processing. For our prototype they are: $N = 32$ and $L = 64$.

Next, applying a 2D discrete Fourier transform, we transformed the signal to the frequency domain:

$$S(p, q) = \sum_{n=1}^{N} \left(\sum_{t=1}^{L} s(t, n) e^{-j2\pi pt/L} \right) e^{-j2\pi qn/N} = \qquad (2)$$

$$= \sum_{i=0}^{I} A^{(i)} \delta(p - w_f^{(i)}, q - w_s^{(i)}) e^{j\phi^{(i)}},$$

where δ is the Dirac delta function, and τ_m is the time delay corresponding to the maximum range. Each ith reflector contributes, to the signal $S(p, q)$, an impulse, in the ideal case, at position

$$w_f^{(i)} = 2\pi k\tau^{(i)}; \quad w_s^{(i)} = 2\pi f_d^{(i)} = 4\pi v^{(i)} \cos\theta^{(i)}/\lambda, \quad (3)$$

where $v^{(i)}$ is the velocity and $\theta^{(i)}$ is the angle between the radar's line of sight and the direction of motion of the object.

The signal $S(p, q)$ of Eq. 2 is referred to as the complex Range-Doppler Map (CRDM). The amplitude term of the CRDM, $|S(p, q)|$, is referred to as the Range-Doppler Map (RDM). The phase term is used to estimate the angle of arrival.

D. Detection

The RDM shows the distribution of energy in each range and Doppler bin. From it, we can detect moving objects that are present in the scene using the CFAR detector [6].

An example RDM with successful detections for a moving hand is illustrated in Fig. 5. Note that while performing a gesture, a moving hand can be considered as a non-rigid object with moving parts that reflect the radar signal independently.

E. Angle estimation

The angle of arrival of an object can be estimated by comparing the signals received at two receivers or from the CRDMs. In our system, we estimate the angle of arrival by comparing the phases of signals received at two receivers as follows:

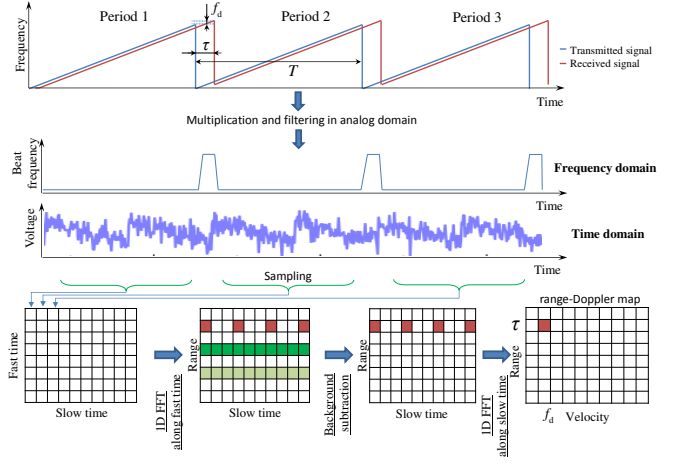$$\theta = \arcsin\left(\frac{\lambda(\angle S_2(p, q) - \angle S_1(p, q))}{2\pi d} \right), \qquad (4)$$

Fig. 4: The range-Doppler processing scheme to measure the Doppler shift (f_d) and the time delay (τ) caused by the motion of an object.
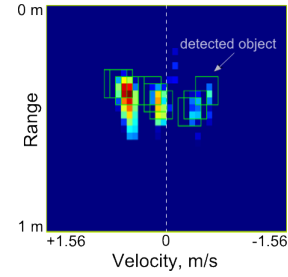

Fig. 5: The RDM of a moving hand. Green squares indicate the detected objects. Since the hand is non-rigid, it appears as a collection of objects in the RDM.

where $\angle$ is the phase extraction operator, d is the physical distance (baseline) between the receiving antennas, and $S_1(p, q)$ and $S_2(p, q)$ are CRDMs at the two receivers.

In our system, we used three receivers in all (Fig. 1). One receiver is positioned in the middle and the other two are displaced horizontally and vertically with respect to it. In this way we estimated the azimuth and elevation angles of the objects. Hence, together with the range measurement, we estimated the position of the object in the spherical coordinate system. Note that we computed the spatial position of only those objects that were detected in the RDM.

The maximum unambiguous angle that can be computed with the phase comparison technique is defined as

$$\theta_{max} = \pm\arcsin(\lambda/2d). \qquad (5)$$

It follows that $d \to \lambda/2$ for the maximum FOV. However, this is not always possible for real systems. For our prototype we achieved the following unambiguous FOV

$$\theta_{max}^{horizontal} = \pm 40°; \quad \theta_{max}^{verical} = \pm 25° \qquad (6)$$

by manually cutting the waveguide antennas to reduce the physical distance between them.

F. Radar parameters selection

The range resolution of the employed range-Doppler estimation is $\Delta r = c/(2B)$, where c is the speed of light and B is the bandwidth of the radar signal. Our system employs the front-end Infineon BGT24MTR12 chip with a bandwidth of $4GHz$ (Fig. 3). Therefore, its range resolution is $\Delta r = 3.75cm$.

The velocity resolution is defined as $\Delta v = c/(2LTf_0)$, where L is the number of accumulated periods and $f_0 = 25GHz$ is the frequency of the carrier. With the selected $L = 64$ we get $\Delta v = 0.05m/s$.

The unambiguous range and velocity values are equal to $r_{max} = cT/2$ and $v_{max} = c/(4Tf_0)$, respectively, where T is the modulation period. For sensing drivers' hand gestures, the maximum distance of interest is $r_{max} = 1.5m$, which results in a modulation period of $T > 100ns$. On the other extreme, assuming the maximum velocity of the hand to be $1.5m/s$ we get $T \leq 2ms$. It is advantageous to select a larger T, to avoid the need for high performance hardware. Therefore, in our system the *chirp period* is set $T = 2ms$.

The output of the radar is a demodulated signal called the beat signal. It's maximum frequency depends on the maximum range as:

$$f_b = \frac{B2r_{max}}{Tc} \approx 19.5KHz. \tag{7}$$

Hence the sampling frequency must be $F_s \geq 39KHz$. We designed analog filters between the radar and the ADC module to reject frequencies $> f_b$.

The estimated frequency of the beat signal f_b results in low performance requirements on components such as analog filters and amplifiers. Additionally the sampling frequency F_s can be realized by low-cost micro-controllers (*e.g.*, the TI Cortex M4F). We sampled both the I and Q channels for one of the receivers (Rx1 in Fig. 1). For the other two receivers we sample only their I channels. In this way we were able to reduce the number of analog circuits that were required, and the amount of information that was transmitted to the PC.

G. Digital signal processing

We performed digital signal processing (Fig. 7) for the radar prototype in two stages. In the first stage, we pre-processed the sampled signal on the micro-controller. In the second stage, we performed the remaining signal processing steps on the PC.

For better efficiency we separated the tasks of control signal generation (for VCO through DAC) and sampling from the signal processing on the micro-controller as shown in Fig. 6. We did this to avoid interference between the interrupts on the micro-controller, and to increase the sampling accuracy.

Since reflections from stationary objects mask the true reflections from the hand, we applied the MTI filter to suppress the contribution of stationary objects. We filtered the sampled demodulated signal at each receiving channel by means of a running average filter as:

$$\hat{s}(t,n) = s(t,n) - B_n(p) \tag{8}$$
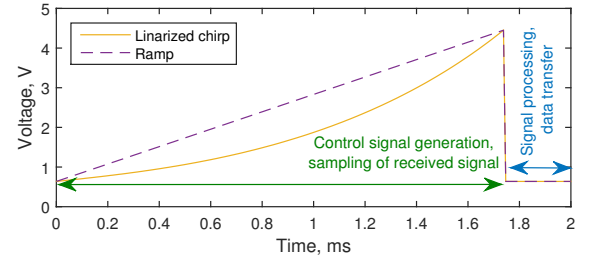$$B_{n+1}(p) = B_n + \alpha\hat{s}(t,n),$$

Fig. 6: The linearized chirp used in the system. It consists of two periods: the actual chirp and the silence part. The former is used for control signal generation and sampling, and the latter is used for signal processing and data transfer.
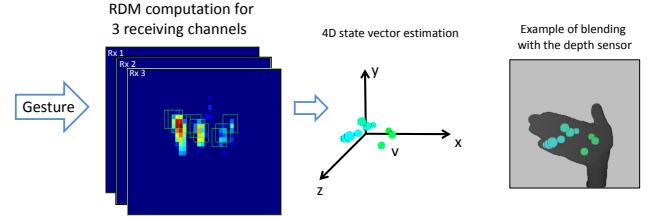

Fig. 7: The 3 receivers of the radar sense the hand gesture. For each receiver, we estimated the RDM and detected moving objects. Additionally, for each detected object, we estimated a 4D vector comprising of spatial coordinates and radial velocity. After calibration, we projected the radar's measurements on to the depth image.

where α is the smoothing factor (selected to be 0.01), and B_n is the background model estimated at time index n. This background subtraction method has low memory and computational requirements, and was implemented on a micro-controller.

Next we applied the first 1D Fourier transform along the fast-time axis. This transformation allowed us to obtain range profiles, which we forwarded to a PC. We compiled a set of range profiles and applied a second 1D Fourier transform along the slow-time axis to compute the RDM. We used overlapping sets of range profiles to compute the RDM, which increases the Doppler resolution. We fit the Gaussian to neighbor cells in RDM for range estimation of detected objects. The fitting allows to get sub-resolution accuracy.

H. Fusion with depth data

The radar system discussed in this paper was part of a larger multi-sensor system, which included an RGB and a depth sensor [5]. Cross-sensor calibration enables information from multiple sensors to be registered and fused. Calibration is required to be performed only once after the relative positions of the sensors is fixed.

We considered two transformation models between 3D points measured by the depth and radar sensors: *linear* and *quadratic*. For both models the transformation was assumed to be:
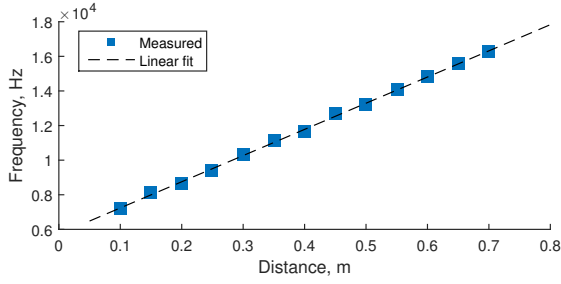
$$P * R = D, \tag{9}$$

Fig. 8: Measurements of the beat frequency for different distances to a stationary metallic disk of diameter $0.18m$.
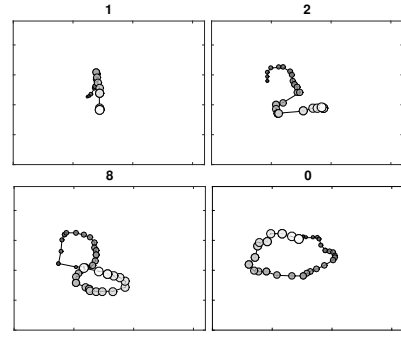

Fig. 10: The trajectories of the hand tracked by our radar system for four dynamic motions: drawing numbers 1, 2, 8 and 0. The first position of the hand is depicted with the smallest dark circle and each subsequent position is represented by a progressively larger circle with higher intensity.

where $D = [X_d \ Y_d \ Z_d]^T$ is a 3D point measured by the depth sensor and P is a transformation (projection) matrix. For the *linear model*, $R = [X_r \ Y_r \ Z_r \ 1]^T$ where the first three dimensions represent the 3D point measured by the radar and P is a matrix of coefficients of size 3×4. For the *quadratic model*, $R = [X_r \ Y_r \ Z_r \ X_r^2 \ Y_r^2 \ Z_r^2 \ 1]^T$ and P is of size 3×7.

We transformed the measurements of the depth sensor (D) to world coordinates as:

$$\hat{X}_d = (X_d - c_x) * Z_d/f_x; \quad \hat{Y}_d = (Y_d - c_y) * Z_d/f_y, \quad (10)$$

where f_x, f_y are the focal lengths of the depth camera, and c_x, c_y are the co-ordinates of its principal point.

To estimate the matrix P, we concurrently observed the 3D coordinates of the center of a moving spherical ball of radius $1.5cm$ with both sensors and estimated the best-fit transformation between them using the linear least squares procedure.

In our system, we placed the depth camera above the radar sensor. We assume the x axis to be along the horizontal direction, the y axis - vertical, and the z axis - optical axis of the depth camera. We use a TOF depth camera (DS325, Softkinetic) with spatial resolution of 320×240 pixels, depth resolution of $\leq 1mm$ and FOV of $74° \times 58°$.

III. EXPERIMENTAL RESULTS

In order to evaluate the reliability our system, we performed the first experiment with a stationary metallic disk of diameter $0.18m$. Then, the background's estimate (Eq. 8) was fixed for all experiments with the stationary disk. The observed relationship between the beat frequency and the distance to the disk is shown in Fig. 8. The strongly linear nature of this relationship is evidence for the high reliability of our system. The standard deviation of the distance measurements was $0.6cm$. The on-board micro-controller performed all measurements by averaging over a period of $2s$. This experiments indicates that our prototype provides reliable measurements of the distance.

Fig. 9 shows the x, y and z coordinates of the calibration ball ($1.5cm$ radius) measured by the depth and radar sensors after cross-sensor calibration with the *quadratic* function. The position of the ball measured by the depth camera can be assumed to be accurate. Overall, the radar is able to follow the ball's position, and provides a reasonable estimate of its spatial location. The histograms of the positional errors are also presented in Fig. 9. They closely resemble zero-mean Gaussian distributions. The standard deviations of errors along the x, y and z axes were $14.2mm$, $11.7mm$ and $16.2mm$, respectively. The *quadratic* transformation model resulted in $0.4mm$, $0.9mm$ and $6.5mm$ lower standard deviations along the x, y and z axes compared to the *linear* model.

Figure 11 shows examples of 10 hand gestures observed by our radar system: 1,2 - fist moving forwards/backwards; 3 - pointing to the side; 4,6 two moving hands; 5 - hand opening; 7,8 thumb motion forwards/backwards; 9 - hand twisting; 10 - calling. Observe that hand gestures are comprised of several micro-motions, which are detected by the radar. The radar estimates the spatial coordinates correctly and even separates the two hands moving with different velocities. It also correctly detects the motion of the thumb.

The radar senses the hand as a non-rigid object and hence reports multiple points for it. The location of these points is not constant and they can be located anywhere within the hand. Therefore, the radar system cannot be relied upon to track the position of the hand very precisely, especially for short ranges, where the hand occupies a significant portion of the FOV (Fig. 11). To track the hand, we instead employed the median of the all the points located on the hand detected by the radar. The results of this tracking methodology are demonstrated in Fig. 10. Notice that the developed radar system can track the hand successfully.

IV. CONCLUSIONS

We presented a short-range FMCW mono-pulse radar system for hand gesture sensing. The radar system estimates the range-Doppler map of dynamic gestures together with the 3D position of the detected hand at 32 FPS. The built prototype radar system successfully measures range and bi-directional radial velocity. The radar estimates the spatial coordinates with a coverage of $\pm 45^0$ and $\pm 30^0$ in the horizontal and vertical directions, respectively. We developed a procedure to jointly calibrate the radar system with a depth sensor. Results of tracking a metallic ball target demonstrate that the radar system is capable of correctly measuring the 3D location of
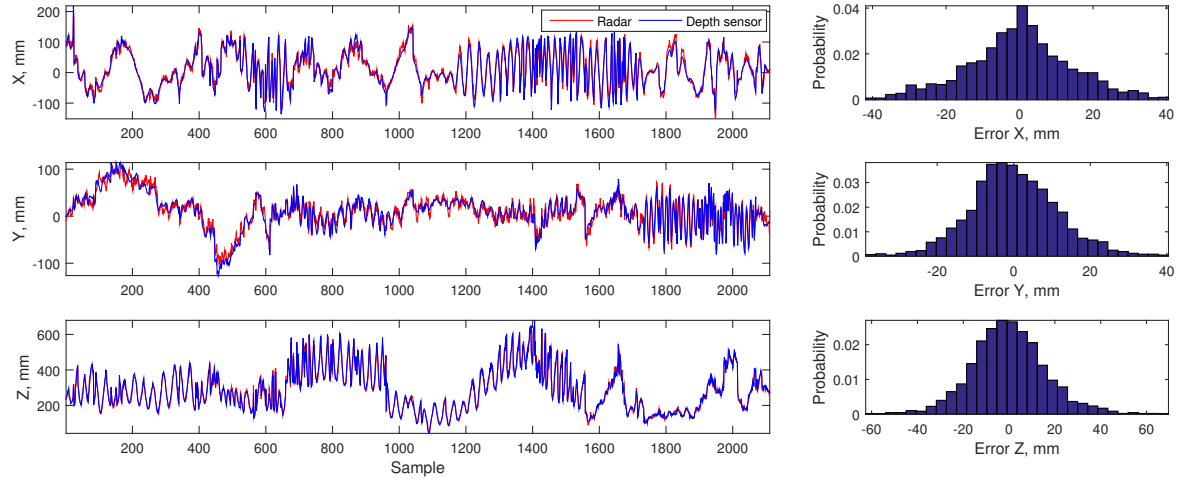
Fig. 9: The 3D positions of the metallic ball measured by the radar and depth sensors (left) after calibration with the *quadratic* function, and the histograms of their positional errors (right).
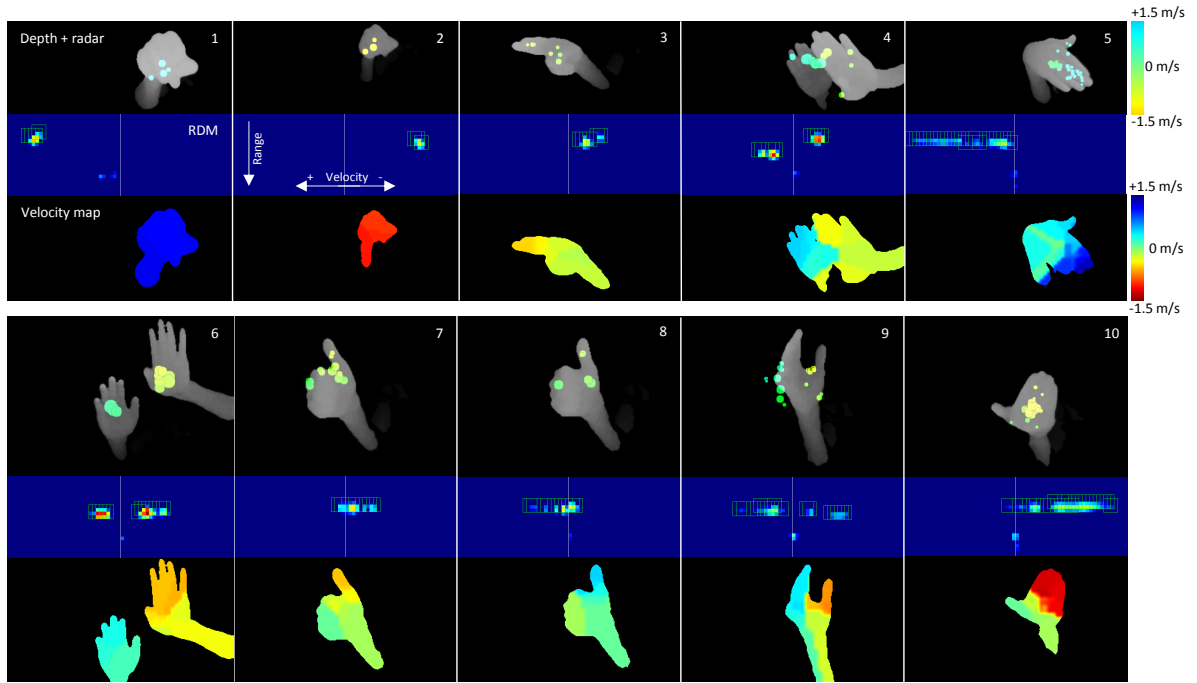

Fig. 11: Dynamic hand gestures observed by the radar. For each gesture, the uppermost image display the points detected by the radar as circles superimposed on a depth image. The color of the circle indicates the velocity of the point. The radius of the circle is proportional the the RCS. The middle image shows the corresponding RDM (see Fig. 5 for description). The lowest image shows the color encoded velocity map of the hand extrapolated from the detected radar points [5].

objects. The experiments on dynamic hand gesture sensing show the reliability of the approach for gesture sensing.

REFERENCES

[1] S. Mitra and T. Acharya, "Gesture recognition: A survey," *IEEE Transactions on Systems, Man, and Cybernetics, Part C: Applications and Reviews*, vol. 37, no. 3, pp. 311–324, 2007.

[2] S. Gupta, D. Morris, S. Patel, and D. Tan, "Soundwave: using the Doppler effect to sense gestures," in *SIGCHI Conference on Human Factors in Computing Systems*, 2012, pp. 1911–1914.

[3] Q. Wan, Y. Li, C. Li, and R. Pal, "Gesture recognition for smart home applications using portable radar sensors," in *IEEE Conference on Engineering in Medicine and Biology Society*, Aug 2014, pp. 6414–6417.

[4] B. Raj, K. Kalgaonkar, C. Harrison, and P. Dietz, "Ultrasonic Doppler sensing in HCI," *IEEE Pervasive Computing*, vol. 11, no. 2, pp. 24–29, Feb 2012.

[5] P. Molchanov, S. Gupta, K. Kim, and K. Pulli, "Multi-sensor system for driver's hand-gesture recognition," in *IEEE Conference on Automatic Face and Gesture Recognition*, May 2015, pp. 1–8.

[6] H. Rohling, "Radar CFAR thresholding in clutter and multiple target situations," *IEEE Transactions on Aerospace and Electronic Systems*, vol. 19, no. 4, pp. 608–621, 1983.